Comparative Study of Temperature-Induced Association of Cyclic and Linear Poly(*N*-isopropylacrylamide) Chains in Dilute Solutions by Laser Light Scattering and Stopped-Flow Temperature Jump

Jing Ye,[†] Jian Xu,[‡] Jinming Hu,[‡] Xiaofeng Wang,[‡] Guangzhao Zhang,[‡] Shiyong Liu,*,[‡] and Chi Wu[†,‡]

Key Laboratory of Soft Matter Chemistry, Department of Polymer Science and Engineering, Hefei National Laboratory for Physical Sciences at the Microscale, University of Science and Technology of China, Hefei, Anhui 230026, China, and Department of Chemistry, The Chinese University of Hong Kong, Shatin, N.T., Hong Kong, China

ABSTRACT: We have comparatively studied the association of *cyclic*- and *linear*-poly(*N*-isopropylacrylamide) (*c*-PNIPAM and *l*-PNIPAM) chains with varying chain lengths and end groups in dilute aqueous solutions by laser light scattering (LLS) and stopped-flow temperature-jump measurements. Dynamic and static LLS results reveal that the heating leads to a microphase transition. The resultant structures of interchain aggregates depend on the heating rate and the chain topologies. In comparison with *l*-PNIPAM chains, a slow heating of *c*-PNIPAM chains in the solution results in stable mesoglobules with a lower average aggregation number, a looser structure, and a smaller average size (∼290 nm). The temperature-jump-induced association of *c*-PNIPAM chains in the stopped-flow measurement reveals two kinetic growth stages, which were tentatively ascribed to the loose packing of contracted *c*-PNIPAM chains and further contraction-induced fragmentation of initially packed *c*-PNIPAM chains due to the lack of interchain entanglements. On the other hand, for *l*-PNIPAM chains, the intrachain contraction and interchain penetration/entanglement simultaneously occur as the temperature increases, leading to larger and more compact aggregates whose size increases with the solution temperature.

Introduction

Thermosensitive water-soluble homopolymers, such as poly(*N*-isopropylacrylamide) (PNIPAM), poly(*N*-vinylcaprolactam) (PVCL), and poly(vinyl methyl ether) (PVME), have been extensively studied in the past two decades due to their unique properties and potential biotechnological applications.[1] Microscopically, the heating can change the conformation of a flexible linear homopolymer chain from an expanded coil to a collapsed globule in a dilute solution as the solvent quality gradually changes from good to poor. Previously, various techniques such as turbidimetry,[2] fluorescence spectroscopy,[3] laser light scattering (LLS),[4–8] and small-angle neutron scattering[9–11] have been employed to study the temperature-dependent conformational change of individual chains as well as interchain association of these thermally sensitive polymers in aqueous solution.

In principle, amphiphilic random copolymers with a proper comonomer distribution on their chain backbones can form stable mesoglobules in dilute solutions,[12–16] but not for linear homopolymers. The latter should form macroscopic precipitates in the two-phase region. However, many previous experiments have shown that linear PNIPAM chains with different lengths can form stable mesoglobules.[1,17] It has been attributed to the amphiphilic nature of NIPAM monomer and the presence of intra- and interchain hydrogen-bonding interactions.

Meanwhile, most efforts have been devoted to some correlation between polymer chain configuration/structure and their properties, in order to search for better performing polymeric materials. Cyclic (or called ring) polymer chains without two free chain ends are a special type of polymer.[18] It is expected that the association of ring polymer chains would involve less entropy change, and it would be much more difficult for them

to undergo interchain entanglements because their two ends are connected together.[19]

Recent improvements of experimental methods render both the synthesis and accurate characterization of cyclic polymers much easier.[20–24] Properties of cyclic and linear chains in good solvents and in melts have been compared.[22–24] In a Θ-solvent, Chu et al.[25] once stated that "the dynamics of cyclic polymer collapse was expected to differ dramatically from the linear chain case because of an important and peculiar role to the chain ends". However, there has been no experimental evidence so far.

Recently, Winnik et al.[24] and our research group[26] independently reported the synthesis of macrocyclic PNIPAM (*c*-PNIPAM) samples via a combination of controlled radical polymerization and "click" reactions. Both research groups reported that *c*-PNIPAM possessed broader thermal phase transition range and prominently lower enthalpy changes (Δ*H*), as compared to linear PNIPAM (*l*-PNIPAM) samples with the same MW. Winnik et al.[24] reported that *c*-PNIPAM exhibited a higher cloud point (CP, 50% transmittance decrease, 1.0 g/L concentration) than the linear counterpart, whereas our results showed that the relative magnitude of CP values of cyclic and linear PNIPAM samples actually depend strongly on polymer concentrations.[26]

In this study, we further investigated differences between the association of linear and cyclic PNIPAM chains in a poor solvent employing dynamic/static LLS and stopped-flow temperature jump techniques. The stability, structure, and growth kinetics of the mesoglobules formed from linear and cyclic PNIPAM samples with varying chain lengths and end groups were systematically examined.

Experimental Section

Materials. *N*,*N*,*N*′,*N*″,*N*″-Pentamethyldiethylenetriamine (PM-DETA, 98%, Aldrich), and copper(I) bromide (CuBr, 99.99%) were purchased from Aldrich and used as received. 2-Bromopropionic

* To whom correspondence should be addressed. E-mail: sliu@ustc.edu.cn.
† The Chinese University of Hong Kong.
‡ University of Science and Technology of China.

Scheme 1. (a) Chemical Structures of *Linear*-PNIPAM$_n$-N$_3$, *Cyclic*-PNIPAM$_n$, and *Triazole*-PNIPAM$_n$; (b) Synthetic Routes for the Preparation of *Triazole*-PNIPAM$_{51}$, Which Can Serve as a Direct Linear Counterpart of *Cyclic*-PNIPAM$_{52}$

linear-PNIPAM$_n$-N$_3$ *cyclic*-PNIPAM$_n$ *triazole*-PNIPAM$_n$

(a)

linear-PNIPAM$_{52}$-Cl   *triazole*-PNIPAM$_{52}$

(b)
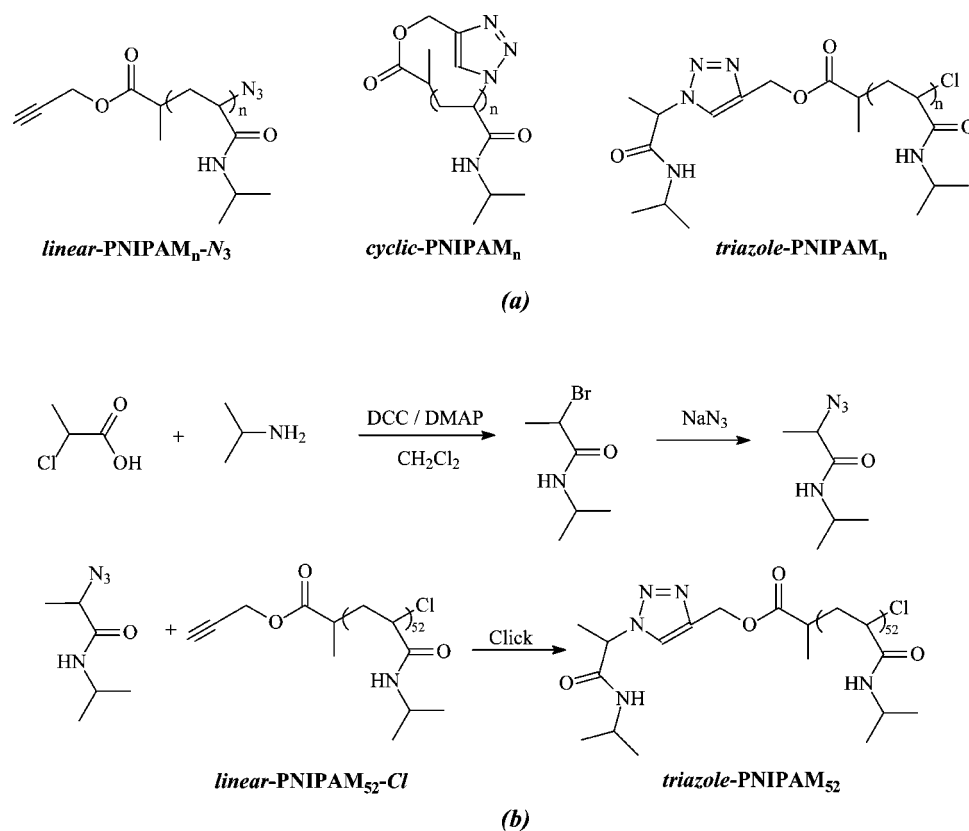
acid (98%) was purchased from ABCR and used as received. Sodium azide (NaN$_3$, 99%) was purchased from Alfa Aesar and used without further purification. *N,N'*-Dicyclohexylcarbodimide (DCC), 4-(dimethylamino)pyridine (DMAP), isopropylamine, and all other chemicals were purchased from Sinopharm Chemical Reagent Co. Ltd. and used as received.

Sample Synthesis. α-Alkyne-ω-azido heterodifunctional PNIPAM precursor (*linear*-PNIPAM-N$_3$) was prepared by atom transfer radical polymerization (ATRP) of *N*-isopropylacrylamide in 2-propanol using propargyl 2-chloropropionate as the initiator. The obtained *linear*-PNIPAM-Cl was reacted with NaN$_3$ to transform the terminal chloride into azide group. The subsequent end-to-end intramolecular coupling reaction under high dilution and "click" conditions leads to efficient preparation of narrow-disperse *cyclic*-PNIPAM. Detailed experimental procedures for the synthesis of *linear*-PNIPAM-N$_3$ and *cyclic*-PNIPAM (Scheme 1a) were reported previously.[26]

The three-step procedures employed for the preparation of *triazole*-PNIPAM, which serves as a direct analogue of *cyclic*-PNIPAM, are shown in Scheme 1b.

Synthesis of N-Isopropyl-2-bromopropionamide. *N*-Isopropyl-2-bromopropionamide was prepared by reacting 2-bromopropionic acid with isopropylamine in the presence of DCC and DMAP. A typical procedure was as follows. A 100 mL round-bottom flask was charged with 2-bromopropionic acid (1.94 g, 12.7 mmol), DCC (2.68 g, 13.0 mmol), and methylene chloride (40 mL). The reaction mixture was cooled to 0 °C in an ice–water bath, and then a mixture of isopropylamine (0.75 g, 12.7 mmol), DMAP (0.2 g), and methylene chloride (10 mL) was added dropwise over a period of 0.5 h under magnetic stirring. After the addition is completed, the reaction mixture was stirred at 0 °C for 1 h and then at room temperature for 12 h. After removing insoluble *N,N'*-dicyclohexylurea by suction filtration, the filtrate was extracted with saturated aqueous solution of NaHCO$_3$ (3 × 50 mL) and acidic water (pH 1, 3 × 50 mL). The organic phase was dried over anhydrous MgSO$_4$ and then evaporated to dryness, affording white solids with a yield of ~81%. ^{1}H NMR (CDCl$_3$, δ, ppm): 6.19 (1H,

N*H*), 4.37 (1H, C*H*Br), 4.04 (1H, NHC*H*), 1.88 (3H, C*H*$_3$CHBr), and 1.20 (6H, CH(C*H*$_3$)$_2$).

Synthesis of N-Isopropyl-2-azidopropionamide. Into a 50 mL round-bottom flask, *N*-isopropyl-2-bromopropionamide (1 g, 5.2 mmol), NaN$_3$ (0.65 g, 10 mmol), and 20 mL of DMF were added. The reaction mixture was allowed to stir at room temperature overnight. After adding methylene chloride (150 mL), the reaction mixture was extracted with deionized water (6 × 50 mL). The organic phase was dried over anhydrous MgSO$_4$ and then evaporated to dryness, affording white needle-shaped crystals with a yield of ~63%. ^{1}H NMR (CDCl$_3$, δ, ppm): 6.14 (1H, N*H*), 4.04 (2H, C*H*N$_3$ and NHC*H*), 1.54 (3H, C*H*$_3$CHN$_3$), and 1.20 (6H, CH(C*H*$_3$)$_2$).

Synthesis of Triazole-PNIPAM. To a Schlenk flask equipped with a magnetic stirring bar, *N*-isopropyl-2-azidopropionamide (31 mg, 0.2 mmol), *linear*-PNIPAM$_{52}$-Cl (0.3 g, 0.05 mmol), and PMDETA (17.3 mg, 0.1 mmol) were added. The flask was carefully degassed by three freeze–pump–thaw cycles, and then CuBr (14.4 mg, 0.1 mmol) was introduced under the protection of nitrogen flow. The flask was sealed under vacuum and placed in an oil bath thermostated at 40 °C. After 20 h, the reaction mixture was precipitated into an excess of anhydrous diethyl ether. The sediments were collected, redissolved in THF, and passed through a neutral alumina column using THF as the eluent to remove copper catalysts. The collected eluents were concentrated and precipitated into an excess of anhydrous diethyl ether. This purification cycle was repeated for three times. The obtained product was dried overnight in a vacuum oven for 24 h (overall yield: 73%; $M_{n,GPC}$ = 8900, M_w/M_n = 1.08).

The structural parameters of *linear*-PNIPAM-N$_3$, *cyclic*-PNIPAM, and *triazole*-PNIPAM samples used in the current study are summarized in Table 1.

Dilute aqueous polymer solutions were prepared by directly dissolving a proper amount of *c*-PNIPAM or *l*-PNIPAM in deionized water separately. The concentrations for laser light scattering (LLS) and stopped-flow measurements are 2 × 10^{-5} and 4 × 10^{-5} g/mL, respectively. To ensure complete dissolution, all the solutions were kept at 4 °C for at least 24 h. The solutions were

Table 1. Properties of Linear and Cyclic Poly(*N*-isopropylacrylamide) Polymers

sample code	$M_{\mathrm{n,GPC}}$[a]	$M_{\mathrm{w}}/M_{\mathrm{n}}$[a]	$M_{\mathrm{n,MALDI}}$[b]	$M_{\mathrm{w}}/M_{\mathrm{n}}$[b]	T_{c}[c] (°C)	CP[c] (°C)
linear-PNIPAM$_{52}$-N_3	8600	1.08	5950	1.05	34	37
cyclic-PNIPAM$_{52}$	7500	1.09	6000	1.04	27	35
linear-PNIPAM$_{260}$-N_3	29400	1.14			32	34
cyclic-PNIPAM$_{260}$	26300	1.16			25	32
triazole-PNIPAM$_{52}$	8900	1.08			38	41

[a] Number-average molecular weight, M_{n}, and polydispersity, $M_{\mathrm{w}}/M_{\mathrm{n}}$, determined by GPC using DMF as eluent. [b] Measured by MALDI-TOF mass spectrometry. [c] The critical phase separation temperature (T_{c}) and the cloud point (CP) were defined as the temperatures corresponding to 1% and 50% decrease of optical transmittance (2.0 g/L aqueous solution) at a wavelength of 500 nm, respectively. The estimated error associated with each value was ±1 °C. It should be noted that the T_{c} value obtained in the current study should be better viewed as the onset temperature of interchain aggregation.

purified by 0.45 μm Millipore (Hydrophilic Millex-LCR PTFE) filters to remove dust particles before each LLS measurement.

Laser Light Scattering. A commercial spectrometer (ALV/DLS/SLS-5022) equipped with a multi-τ digital time correlator (ALV5000) and a cylindrical 22 mW UNIPHASE He−Ne laser ($\lambda_0 = 632$ nm) as the light source was used. The incident beam was vertically polarized with respect to the scattering plane. The details of our LLS instrument and theory can be found elsewhere.[27] In dynamic LLS, the Laplace inversion of each measured intensity−intensity time correlation function $G^{(2)}(q,t)$ in the self-beating mode can lead to a line-width distribution $G(\Gamma)$.[28,29] For a pure diffusive relaxation, Γ is related to the translational diffusion coefficient D by $(\Gamma/q^2)_{c\to0,q\to0} \to D$ or further to the hydrodynamic radius R_{h} via the Stokes−Einstein equation, $R_{\mathrm{h}} = k_{\mathrm{B}}T/(6\pi\eta_0 D)$, where k_{B}, T, and η_0 are the Boltzmann constant, the absolute temperature, and the solvent viscosity, respectively. In dynamic LLS, the scattering angle was fixed at 17.5°.

In static LLS, we can obtain the weight-average molar mass (M_{w}) and the z-average root-mean square radius of gyration ($\langle R_{\mathrm{g}}^2 \rangle_z^{1/2}$ or written as $\langle R_{\mathrm{g}} \rangle$) of scattering objects in a dilute solution or dispersion from the angular dependence of the excess absolute scattered intensity, known as the Rayleigh ratio $R_{vv}(q)$, on the basis of eq 1.

$$\left(\frac{KC}{R_{vv}(q)}\right)_{c\to0} \cong \frac{1}{M_{\mathrm{w}}}\left(1 + \frac{1}{3}\langle R_{\mathrm{g}}^2\rangle_z q^2\right) \quad \text{for } q\langle R_{\mathrm{g}}^2\rangle^{1/2} < 1 \quad (1)$$

For larger particles with $q\langle R_{\mathrm{g}}^2\rangle^{1/2} > 1$, the Guinier approximation (eq 2) was employed for simplicity:

$$\left(\frac{KC}{R_{vv}(q)}\right)_{c\to0} \cong \frac{1}{M_{\mathrm{w}}}\exp\left(\frac{1}{3}\langle R_{\mathrm{g}}^2\rangle_z q^2\right) \quad \text{for large particles} \quad (2)$$

where $K = 4\pi^2 n^2(\mathrm{d}n/\mathrm{d}C)^2/(N_A\lambda_0^4)$ and $q = (4\pi n/\lambda_0)\sin(\theta/2)$ with N_A, $\mathrm{d}n/\mathrm{d}C$, n, and λ_0 being the Avogadro number, the specific refractive index increment, the solvent refractive index, and the wavelength of the light in vacuum, respectively. In the temperature range of 25−66 °C, each polymer solution was heated inside the LLS spectrometer. Each step of the increase of temperature was 2−3 °C. The temperature stability is ±0.05 °C. All the LLS measurements were carried out after the temperature reached its equilibrium. The $\mathrm{d}n/\mathrm{d}C$ value of 0.167 mL/g for PNIPAM at 25 °C was used to calculate the weight-average molar mass (M_{w}),[30] and it varies little with the solution temperature.[31] Considering the overall absolute uncertainty of static LLS, we can safely neglect a small uncertainty introduced by a slight change of $\mathrm{d}n/\mathrm{d}C$ at higher temperatures.

Stopped-Flow with Light Scattering Detection. Stopped-flow studies were carried out using a Bio-Logic SFM300/S stopped-flow instrument. The SFM-3/S is a three-syringe (10 mL) instrument in which all step-motor-driven syringes (S1, S2, S3) can be operated independently to carry out single or double mixing. The SFM-300/S stopped-flow device is attached to the MOS-250 spectrometer; kinetic data were fitted using the Biokine program (Bio-Logic kinetic data were fitted using the program Biokine (Bio-Logic).
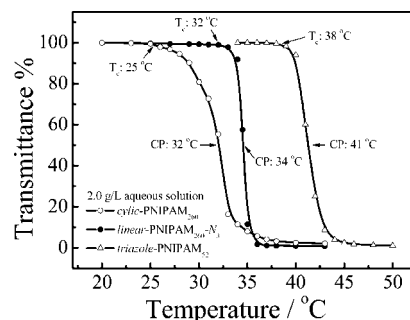

Figure 1. Temperature dependences of optical transmittance at 500 nm obtained for 2.0 g/L aqueous solutions of *linear*-PNIPAM$_{260}$-N_3, *cyclic*-PNIPAM$_{260}$, and *triazole*-PNIPAM$_{52}$. The critical phase separation temperature (T_{c}) and cloud point (CP) were defined as the temperatures corresponding to 1% and 50% decrease of transmittance, respectively.

For the light scattering detection at a scattering angle of 90°, both the excitation and emission wavelengths were adjusted to 335 nm with 10 nm slits. The typical dead time of FC-15 flow cell is 2.6 ms.

The millisecond temperature jump (mT-jump) accessory is equipped with a standard Bio-Logic stopped-flow observation cell; three thermoelectric Peltier elements are used to control the initial temperatures of the two solutions and that of the observation cell after mixing. The temperature of the mixed solution was calibrated to be the same as the observation cell (Peltier controlled) with the aid of a thermosensitive fluorescent dye, *N*-acetyl-L-tryptophanamide (NATA). The precision of the temperature jump is within ±0.1 °C, and the temperature stability in the observation cell after temperature jump was <1%.[32] At each final target temperature, at least 10 shots were done consecutively. The results were quite reproducible, and an average of these kinetic traces was employed at each temperature.

Results and Discussion

Recently, Stöver et al.[33,34] successfully synthesized a series of narrow-disperse PNIPAM with varying MWs and end groups by ATRP and reported that the CPs can vary in the broad range of 32−70 °C, depending on their MWs and the hydrophobicity of end groups. We have established previously[26] that the critical phase separation temperature (T_{c}, onset temperature of interchain aggregation) of *cyclic*-PNIPAM$_{52}$ is systematically lower than that of *linear*-PNIPAM$_{52}$-N_3 in the concentration range of 0.2−2.0 g/L, and the former possess much larger polymer concentration dependences. At polymer concentrations of 2.0 and 0.2 g/L, T_{c} values of *cyclic*-PNIPAM$_{52}$ are 27 and 38 °C, and those of *linear*-PNIPAM$_{52}$ are 34 and 39 °C, respectively.

In the current study, three samples (*triazole*-PNIPAM$_{52}$, *linear*-PNIPAM$_{260}$-N_3, and *cyclic*-PNIPAM$_{260}$; Scheme 1a) were newly synthesized. Bearing a NIPAM end group and a triazole moiety, *triazole*-PNIPAM$_{52}$ serve as a direct linear counterpart of *cyclic*-PNIPAM$_{52}$; thus, the effects of end-group amphiphilicity on the phase transition of *linear*-PNIPAM$_{52}$-N_3 and *triazole*-PNIPAM$_{52}$ samples can be elucidated. From Figure 1, we can tell that T_{c} of *triazole*-PNIPAM$_{52}$ is much higher (38 °C) than that of *linear*-PNIPAM$_{52}$-N_3 (34 °C). This is reasonable considering that triazole moiety in *triazole*-PNIPAM$_{52}$ is highly hydrophilic.[33,34]

Figure 1 also shows the temperature-dependent transmittance of the aqueous solutions of *cyclic*-PNIPAM$_{260}$ and *linear*-PNIPAM$_{260}$-N_3, exhibiting T_{c} values of 25 and 32 °C, respectively. The T_{c} and CP values of all five samples linear and cyclic samples with varying chain lengths and end groups are summarized in Table 1. As the chain length of *cyclic*-PNIPAM increases from 52 to 260, the T_{c} value decreases from 27 to 25 °C. This is similar to those observed for linear PNIPAM

samples bearing the same end groups.[33,34] After elucidating the effects of end groups and chain lengths on the phase transition of cyclic and linear PNIPAM chains, we can now safely conclude from Table 1 that the T_c of the former is systematically lower than the latter.

Since 1950s, the hydrophobic effect has been received much attention and widely discussed.[35,36] Later on, it has been generally recognized that the classic Flory−Huggins theory which successfully predicts the upper critical solution temperature (UCST) phase transition of polymers in organic solvents fails to explain the LCST (lower critical solution temperature) transitions in aqueous solution, which is mainly due to the involvement of entropy changes of water molecules induced by the hydrophobic effect.

Generally speaking, for systems with LCST, both hydrophilicity and hydrophobicity should be taken into account when phase separation is considered.[37,38] In aqueous solution of polymers exhibiting the LCST-type phase transition, the hydrophobic effect consists of restructuring of water molecules near nonpolar moieties in terms of hydrophobic hydration and in the mutual interaction and association of nonpolar polymer segments (hydrophobic interaction). An increase of solution temperature will result in a reduction of total number of structured water molecules around the hydrophobic moiety but strengthen the hydrophobic interaction. Thus, the loss of entropy for solutes could be superimposed by the positive entropy change of solvent molecules due to the dissociation of bounded water molecules so that the total translational entropy increases, which leads to the phase separation consequently.

Note that *c*-PNIPAM chains have less conformational entropy in the swollen state than *l*-PNIPAM chains. Therefore, during the swollen-to-collapse transition, *c*-PNIPAM chains lose less conformational entropy than *l*-PNIPAM chains. As discussed before, this negative change of conformational entropy is compensated by a larger positive change of translational entropy of water molecules. The overall entropy change for *c*-PNIPAM chains is more positive so that it requires a lower phase transition temperature to make the change of free energy to be negative.

Meanwhile, in the vicinity of nonpolar moieties, the mobility of water molecules is highly reduced due to the formation of cagelike structures among them.[39,40] Compared to *l*-PNIPAM chains, during the process of hydrophobic hydration, water molecules are much less structured and more mobile in the vicinity of *c*-PNIPAM chains mainly due to the chain connectivity and topology; i.e., the steric constraints existing for cyclic chains will arrest the formation of hydration structures to a large extent considering the orientations of hydrogen bonds. Therefore, hydrogen bonds formed around of *l*-PNIPAM chains are stronger and more stable against perturbations and destructions. The above discussions could safely account for both the higher phase transition temperature and larger ΔH of *l*-PNIPAM in comparison with its cyclic counterpart.

Figure 2 shows the temperature dependence of the average aggregation number, $\langle N_{agg} \rangle$, for *cyclic*-PNIPAM$_{52}$ and *linear*-PNIPAM$_{52}$-N_3 in aqueous solutions at a concentration of 2×10^{-5} g/mL, where $\langle N_{agg} \rangle$ is calculated from the ratio of the weight-average molar masses of the resultant aggregates and individual polymer chains (unimers). Guinier plots obtained for aggregates formed from *cyclic*-PNIPAM$_{52}$ and *linear*-PNIPAM$_{52}$-N_3 at different temperatures are shown in Figures S1 and S2 in the Supporting Information. Note that in LLS the scattered light intensity (*I*) is proportional to the square of the molar mass of a scattering object (*M*), i.e., $I \propto M^2$. As shown in Figure 2, the average molar mass of the PNIPAM aggregates are 6 orders of magnitude higher than those of individual PNIPAM chains. Therefore, the scattered light intensity from individual chains is insignificant in comparison with that from larger aggregates.
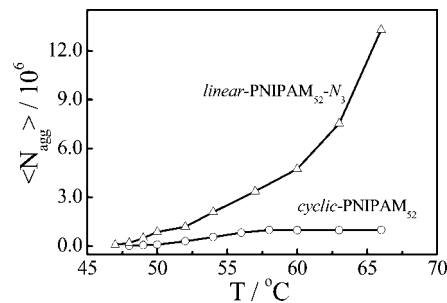

Figure 2. Temperature dependence of average aggregation number, $\langle N_{agg} \rangle$, of mesoglobules of *cyclic*-PNIPAM$_{52}$ and *linear*-PNIPAM$_{52}$-N_3 formed during a slow heating process, where $\langle N_{agg} \rangle = M_{w,agg}/M_{w,chain}$ with $M_{w,agg}$ and $M_{w,chain}$ the weight-average molar masses of the aggregates and the chains, respectively. Each data point was obtained after the temperature equilibrium was reached.
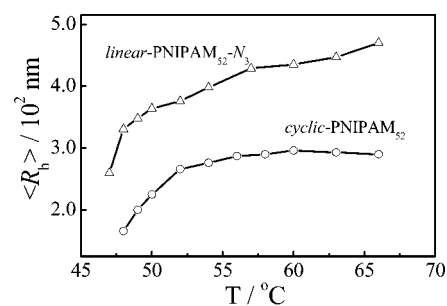

Figure 3. Temperature dependence of average hydrodynamic radius, $\langle R_h \rangle$, of mesoglobules of *cyclic*-PNIPAM$_{52}$ and *linear*-PNIPAM$_{52}$-N_3 formed during a slow heating process. Each data point was obtained after the temperature equilibrium was reached.

For *cyclic*-PNIPAM$_{52}$ and *linear*-PNIPAM$_{52}$-N_3, the temperature-dependent $\langle N_{agg} \rangle$ curves exhibit inflection point at ∼46 and ∼47 °C, indicating the microphase transition as the temperature increases in the range of 25−66 °C. In the current case, the obtained relatively high T_c values of *cyclic*-PNIPAM$_{52}$ and *linear*-PNIPAM$_{52}$-N_3 (46 and 47 °C) can thus be ascribed to the quite low polymer concentrations (2×10^{-5} g/mL), and we have previously established that the T_c of cyclic and linear PNIPAM has strong concentration dependences.[26]

As expected, $\langle N_{agg} \rangle = 1$ before the solution reaches its microphase transition temperature for both *cyclic*-PNIPAM$_{52}$ and *linear*-PNIPAM$_{52}$-N_3. Above T_c, they behave distinctively. Namely, $\langle N_{agg} \rangle$ of *cyclic*-PNIPAM$_{52}$ aqueous solution gradually increases and reaches a constant plateau (∼9×10^5) at ∼58 °C, while $\langle N_{agg} \rangle$ of *linear*-PNIPAM$_{52}$-N_3 continuously increases with the solution temperature. At ∼58 °C, $\langle N_{agg} \rangle$ of *linear*-PNIPAM$_{52}$-N_3 reaches ∼4.5×10^6, which is ca. 5 times larger than that of *cyclic*-PNIPAM$_{52}$ at the same temperature.

Figure 3 shows the temperature dependence of the average hydrodynamic radius, $\langle R_h \rangle$, of *cyclic*-PNIPAM$_{52}$ and *linear*-PNIPAM$_{52}$-N_3 in aqueous solutions. Note that before reaching the microphase transition temperature $\langle R_h \rangle$ could not be measured because we were not able to get a sufficient scattered intensity from such a dilute solution (2×10^{-5} g/mL) of short PNIPAM chains ($M_n \sim 6000$ g/mol). The temperature dependence of $\langle R_h \rangle$ has a similar tendency as that of $\langle N_{agg} \rangle$ shown in Figure 2. For *cyclic*-PNIPAM, $\langle R_h \rangle$ increases with the solution temperature and approaches a constant plateau (∼290 nm) at ∼58 °C. It should be stated that such formed aggregates at temperatures higher than 58 °C are so stable that there was no change in either $\langle N_{agg} \rangle$ or $\langle R_h \rangle$ over a few days. In contrast, for *linear*-PNIPAM$_{52}$-N_3, $\langle R_h \rangle$ continuously increases with the solution temperature. A combination of Figures 1 and 2 reveals that *cyclic*-PNIPAM$_{52}$ chains can form stable mesoglobules with
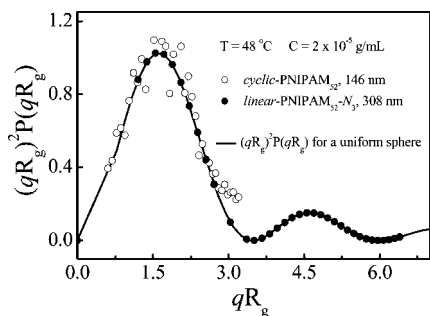
Figure 4. Comparison of Kratky plot of a uniform sphere particle with experimental qR_g-dependent $(qR_g)^2 P(qR_g)$ for both *cyclic*-PNIPAM$_{52}$ and *linear*-PNIPAM$_{52}$-N_3 chains in aqueous solution.
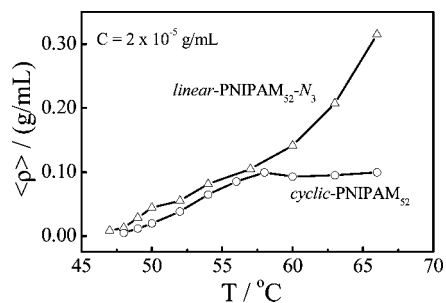

Figure 5. Temperature dependence of average chain density, $\langle\rho\rangle$, of PNIPAM mesoglobules formed in a slow heating process, where $\langle\rho\rangle$ is defined as $M_w/N_A[(4/3)\pi\langle R_h\rangle^3]$.

a limited number of chains at higher temperatures, and their average sizes are much smaller. Note that in the current LLS experimental setup $\lambda = 632$ nm and scattering angle was in the range of $15°–150°$. The precisely measurable range of $\langle R_g\rangle$ is $\sim30–300$ nm. As shown in Figure 3, even at the initial stage of aggregation ($T = 48$ °C), $\langle R_h\rangle$ of the aggregates made of *linear*-PNIPAM already reaches ~300 nm. Considering the limited precision, we did not use the values of $\langle R_g\rangle$ for detailed discussion.

In order to further check that the resultant aggregates have a spherical structure, a Kratky plot of $(q^2R_g^2)P(qR_g)$ vs qR_g is shown in Figure 4. It has been known that for a uniform hard sphere[27,28] $P(qR_g) = [3x^{-3}(\sin x - x \cos x)]^2$ with $x = (5R_g^2/3)^{1/2}$. Figure 4 clearly shows that the experimental points are well represented by $(q^2R_g^2)P(qR_g)$ for a uniform sphere for both *cyclic*-PNIPAM$_{52}$ and *linear*-PNIPAM$_{52}$-N_3 aggregates, namely, the heating results in mesoglobules.[14]

On the basis of their spherical structures, we can further calculate the temperature dependence of the average chain density, $\langle\rho\rangle$, of the aggregates, defined as $M_w/[N_A(4/3)\pi\langle R_h\rangle^3]$, for both *cyclic*-PNIPAM$_{52}$ and *linear*-PNIPAM$_{52}$-N_3. Figure 5 shows that, for *cyclic*-PNIPAM$_{52}$, $\langle\rho\rangle$ increases with the solution temperatures and approaches a constant plateau (~0.08 g/cm³), indicating a very loose structure. On the other hand, for *linear*-PNIPAM$_{52}$-N_3, $\langle\rho\rangle$ continuously increases with the temperature and reaches ~0.30 g/cm³ at 66 °C, reflecting that aggregates made of *linear*-PNIPAM$_{52}$-N_3 are denser. There is no plateau of $\langle\rho\rangle$ for *linear*-PNIPAM$_{52}$-N_3. As PNIPAM chains used contains ~52 monomer units and ~20 Kohn segments, which can lead to certain flexibility with an average end-to-end distance of ~3.5 nm. To further elucidate the effect of chain length and consequently the chain flexibility on the aggregation behavior, static and dynamic LLS studies were also conducted for *cyclic*-PNIPAM$_{260}$ and *linear*-PNIPAM$_{260}$-N_3. The results follow similar trends as those obtained for *cyclic*-PNIPAM$_{52}$ and *linear*-PNIPAM$_{52}$-N_3.

The continuous increase of $\langle\rho\rangle$ with the temperature signals further interchain penetration. In contrast, the presence of a
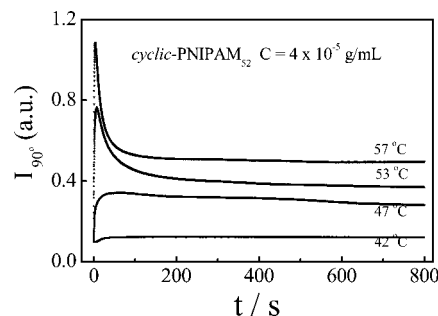

Figure 6. Time dependences of scattered light intensities of *cyclic*-PNIPAM$_{52}$ in aqueous solution after an abrupt temperature jump from 35 °C to different final temperatures in a stopped-flow device. The final polymer concentrations were fixed at 4×10^{-5} g/mL.

plateau for *c*-PNIPAM shows that after the chain is fully contracted the insertion of additional chains into each existing aggregate or the merge of two aggregates stops because it is more difficult for ring-shaped polymer chains without chain ends to interpenetrate with each other. This explains why the mesoglobules made of *c*-PNIPAM chains have a much lower density (0.08 g/cm³) than those made of *l*-PNIPAM chains.

The discrepancy between the association behavior of *l*-PNIPAM and *c*-PNIPAM chains in water above T_c should be due to the suppression of interchain entanglement of *c*-PNIPAM chains without two free chain ends, or in other words, the existence of repulsive forces between cyclic polymer chains resulted from the topological prohibition of interchain linking. Therefore, stable mesoglobules made of *c*-PNIPAM chains can be viewed as a simple packing of individual collapsed single chain globules, just like the aggregation of small colloidal particles.

Heating the solution in the LLS spectrometer in a step-by-step fashion can be considered as an infinite slow process. In order to check the effect of the heating rate, we further used a stopped-flow temperature-jump device with a light-scattering detection to comparatively study the association of *c*-PNIPAM and *l*-PNIPAM in water. In such a study, we can also obtain the mesoglobule growth kinetics, which has been received much less attention.[41–43] In the stopped-flow device, we are able to jump the solution temperature from 35 °C to different final temperatures within less than 1 ms. The temperature jump is realized by mixing a polymer solution at 35 °C with hot water at a preset temperature. The final polymer concentration was fixed at 4×10^{-5} g/mL after stopped-flow mixing.

Figures 6 and 7 respectively show the association kinetics of *cyclic*-PNIPAM$_{52}$ and *linear*-PNIPAM$_{52}$-N_3 chains after the temperature jump in terms of the change of the scattered intensity. It is really surprising to see that for *cyclic*-PNIPAM$_{52}$ the interchain aggregation has more than one stage depending on the final temperatures. In the final temperature range of $42–47$ °C, the scattered intensity increases initially with time and approaches a plateau, indicating a simple interchain association. While in the range $53–57$ °C, the scattered intensity sharply increases within the first $15–20$ ms after the temperature jump and then quickly decays to a constant value. The initial intensity increase of can be ascribed to interchain association, whereas the subsequent intensity decrease suggests the fragmentation of initial aggregates, presumably due to intrachain contraction of individual ring chain and the lack of interchain entanglement. For the observed scattered intensity maximum during the growth of mesoglobules of *c*-PNIPAM, an alternate explanation is that the initially formed loose aggregates might collapse at a constant aggregation number. For large particles ($qR_g \gg 1$) in the dilute solution, the scattered light intensity at 90° is very sensitive to particle sizes and will typically exhibit
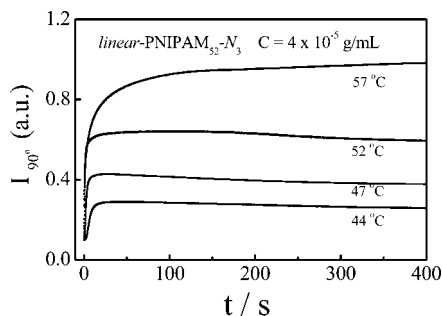
Figure 7. Time dependences of scattered light intensities of *linear*-PNIPAM$_{52}$-N_3 in aqueous solution after an abrupt temperature jump from 35 °C to different final temperatures in a stopped-flow device. The final polymer concentrations were fixed at 4×10^{-5} g/mL.
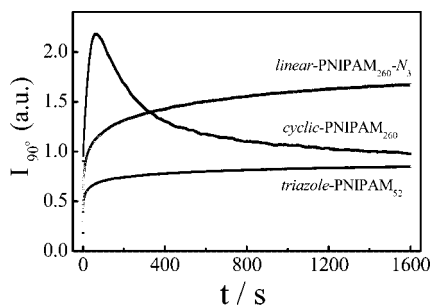

Figure 8. Time dependences of scattered light intensities of *triazole*-PNIPAM$_{52}$, *linear*-PNIPAM$_{260}$-N_3, and *cyclic*-PNIPAM$_{260}$ in aqueous solution after an abrupt temperature jump from 35 to 57 °C in a stopped-flow device. The final polymer concentrations were fixed at 4×10^{-5} g/mL.

an intensity oscillation with the change of them. However, we tentatively speculate that the latter mechanism is less probable due to the following two reasons: (1) only one scattered intensity maximum was observed; (2) the polydisperse nature of aggregates tend to smear intensity oscillations with the reduction of particle sizes. However, we cannot completely exclude the second mechanism at the current stage.

For *linear*-PNIPAM$_{52}$-N_3, each temperature jump leads to an expected monotonic increase of the scattered intensity with time before it approaches a constant after $\sim$200–300 s. The final scattered intensity increases with the final temperature after the mixing, which is consistent with that observed in the slow heating mode during LLS measurements. This indicates that more chains can aggregate together at a higher temperature.

In general, the different mesoglouble growth kinetics between *cyclic*-PNIPAM$_{52}$ and *linear*-PNIPAM$_{52}$-N_3 might have two alternate interpretations, i.e., polymer topology or the end group effects. To elucidate which factor dominates the different aggregation processes between cyclic and linear samples, we further studied the growth kinetics of *triazole*-PNIPAM$_{52}$, *cyclic*-PNIPAM$_{260}$, and *linear*-PNIPAM$_{260}$-N_3 mesogloubles upon a stopped-flow temperature jump (Figure 8). We can clearly see that although *triazole*-PNIPAM$_{52}$ bears a highly hydrophilic triazole moiety, its aggregation kinetics is much similar to that of *linear*-PNIPAM$_{52}$-N_3, and no maximum in scattered light intensities can be found. Thus, the end-group amphiphilicity of linear PNIPAM chains exhibit no discernible effects on its aggregation behavior.

Upon further increasing the chain lengths of *c*-PNIPAM from 52 to 260, the effect of end group, if any, on their aggregation properties will significantly diminish. We can observe from Figure 8 that the growth kinetics of *cyclic*-PNIPAM$_{260}$ follows similar trends to that of *cyclic*-PNIPAM$_{52}$; the scattered intensity abruptly increases to a maximum and then gradually decreases
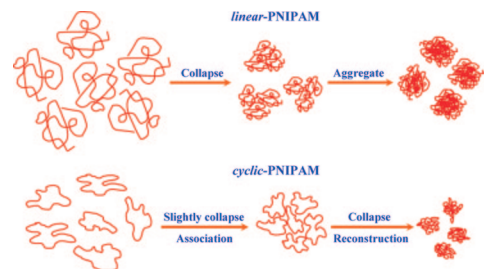

Figure 9. Schematic illustrations for the formation of stable mesoglobules from *c*-PNIPAM and *l*-PNIPAM chains during the fast heating process.

to plateau value. A comparison of the aggregation kinetics of *cyclic*-PNIPAM$_{260}$ and *cyclic*-PNIPAM$_{52}$ (Figures 6 and 8) further tells us that the former is much slower. For *cyclic*-PNIPAM$_{52}$ chains, the scattered intensity maximum appears at $\sim$5 s, and it levels off after $\sim$150 s upon a temperature jump from 35 to 57 °C; whereas for *cyclic*-PNIPAM$_{260}$, the two characteristic time scales are $\sim$60 and >1500 s, respectively. A reasonable interpretation needs to be further explored. From results shown in Figures 6–8 we can at least conclude that the topology difference between cyclic and linear PNIPAM chains dominates their contrasting aggregation properties.

Conclusion

A comparative study of the association of linear and cyclic poly(*N*-isopropylacrylamide) (*l*-PNIPAM and *c*-PNIPAM) chains with varying chain lengths and end groups, respectively, in the slow and fast heating processes shows that the initial chain configuration (topology) exerts a huge effect on how these PNIPAM chains can aggregate together to form stable mesoglobules in dilute aqueous solutions. When the solution is heated above the microphase transition temperature (T_p), *l*-PNIPAM chains simultaneously undergo intrachain contraction and interchain association/entanglement to form large and dense aggregates whose size increases with the solution temperature. In contrast, *c*-PNIPAM chains tend to form smaller and stable mesoglobules with a relatively lower chain density, presumably due to the lack of interchain entanglement and penetration. The fast heating on a stopped-flow temperature-jump device shows that a sudden heating of *c*-PNIPAM chains in a dilute solution to temperatures higher than T_p initially leads to large, unstable, and loose aggregates that subsequently undergo fragmentation, resulting in smaller and stable mesoglobules made of individual collapsed single-chain globules. Figure 9 schematically summarizes the differences in the association of linear and cyclic PNIPAM chains in dilute solutions.

Supporting Information Available: Guinier plots obtained for aggregates formed from *cyclic*-PNIPAM$_{52}$ and *linear*-PNIPAM$_{52}$-N_3 at different temperatures. This material is available free of charge via the Internet at http://pubs.acs.org.

References and Notes

(1) Aseyev, V.; Hietala, S.; Laukkanen, A.; Nuopponen, M.; Confortini, O.; Du Prez, F. E.; Tenhu, H. *Polymer* **2005**, *46*, 7118–7131.
(2) Schild, H. G. *Prog. Polym. Sci.* **1992**, *17*, 163–249.
(3) Winnik, F. M. *Polymer* **1990**, *31*, 2125–2134.
(4) Wu, C.; Zhou, S. Q. *Phys. Rev. Lett.* **1996**, *77*, 3053–3055.
(5) Wu, C.; Wang, X. H. *Phys. Rev. Lett.* **1998**, *80*, 4092–4094.

(6) Kubota, K.; Fujishige, S.; Ando, I. *J. Phys. Chem.* **1990**, *94*, 5154–5158.

(7) Wang, X. H.; Wu, C. *Macromolecules* **1999**, *32*, 4299–4301.

(8) Wang, X. H.; Qiu, X. P.; Wu, C. *Macromolecules* **1998**, *31*, 2972–2976.

(9) Lee, L. T.; Cabane, B. *Macromolecules* **1997**, *30*, 6559–6566.

(10) Muller, F.; Delsanti, M.; Auvray, L.; Yang, J.; Chen, Y. J.; Mays, J. W.; Deme, B.; Tirrell, M.; Guenoun, P. *Eur. Phys. J. E* **2000**, *3*, 45–53.

(11) Muller, F.; Guenoun, P.; Delsanti, M.; Deme, B.; Auvray, L.; Yang, J.; Mays, J. W. *Eur. Phys. J. E* **2004**, *15*, 465–472.

(12) Timoshenko, E. G.; Kuznetsov, Y. A. *Europhys. Lett.* **2001**, *53*, 322–327.

(13) Timoshenko, E. G.; Kuznetsov, Y. A. *J. Chem. Phys.* **2000**, *112*, 8163–8175.

(14) Siu, M. H.; Liu, H. Y.; Zhu, X. X.; Wu, C. *Macromolecules* **2003**, *36*, 2103–2107.

(15) Siu, M. H.; He, C.; Wu, C. *Macromolecules* **2003**, *36*, 6588–6592.

(16) Kujawa, P.; Tanaka, F.; Winnik, F. M. *Macromolecules* **2006**, *39*, 3048–3055.

(17) Gorelov, A. V.; DuChesne, A.; Dawson, K. A. *Physica A* **1997**, *240*, 443–452.

(18) Semlyen, E. R. *Cyclic Polymers*, 2nd ed.; Kluwer Academic Publishers: New York, 2000.

(19) Di Marzio, E. A.; Guttman, C. M. *Macromolecules* **1987**, *20*, 1403–1408.

(20) Brown, S.; Szamel, G. *J. Chem. Phys.* **1998**, *109*, 6184–6192.

(21) Cifre, J. G. H.; Pamies, R.; Martinez, M. C. L.; de la Torre, J. G. *Polymer* **2005**, *46*, 267–274.

(22) Bensafi, A.; Maschke, U.; Benmouna, M. *Polym. Int.* **2000**, *49*, 175–183.

(23) Roland, C. M.; Ngai, K. L.; Santangelo, P. G.; Qiu, X. H.; Ediger, M. D.; Plazek, D. J. *Macromolecules* **2001**, *34*, 6159–6160.

(24) Qiu, X. P.; Tanaka, F.; Winnik, F. M. *Macromolecules* **2007**, *40*, 7069–7071.

(25) Chu, B.; Ying, Q. C.; Grosberg, A. Y. *Macromolecules* **1995**, *28*, 180–189.

(26) Xu, J.; Ye, J.; Liu, S. Y. *Macromolecules* **2007**, *40*, 9103–9110.

(27) Teraoka, I. *Polymer Solution*; John Wiley & Sons: New York, 2002.

(28) Chu, B. *Laser Light Scattering*, 2nd ed.; Academic Press: New York, 1991.

(29) Berne, B. J.; Pecora, R. *Dynamic Light Scattering*; Plenum Press: New York, 1976.

(30) Zhou, S. Q.; Fan, S. Y.; Auyeung, S. C. F.; Wu, C. *Polymer* **1995**, *36*, 1341–1346.

(31) Kujawa, P.; Tanaka, F.; Winnik, F. M. *Macromolecules* **2006**, *39*, 3048–3055.

(32) Zhang, Y. F.; Wu, T.; Liu, S. Y. *Macromol. Chem. Phys.* **2007**, *208*, 2492–2501.

(33) Xia, Y.; Yin, X.; Burke, N.; Stover, H. *Macromolecules* **2005**, *38*, 5937–5943.

(34) Xia, Y.; Burke, N.; Stover, H. *Macromolecules* **2006**, *39*, 2275–2283.

(35) Tanford, C. *The Hydrophobic Effect*; Wiley-Interscience: New York, 1980.

(36) Ben-Naim, A. *Hydrophobic Interactions*; Plenum Press: New York, 1980.

(37) Otake, K.; Inomata, H.; Konno, M.; Saito, S. *Macromolecules* **1990**, *23*, 283.

(38) Inomata, H.; Goto, S.; Saito, S. *Macromolecules* **1990**, *23*, 4887.

(39) Tamai, Y.; Tanaka, H.; Nakanishi, K. *Macromolecules* **1996**, *29*, 6750.

(40) Maeda, Y.; Tsukida, N.; Kitano, H.; Terada, T.; Yamanaka, J. *J. Phys. Chem.* **1993**, *97*, 13903.

(41) Kuznetsov, Y. A.; Timoshenko, E. G.; Dawson, K. A. *J. Chem. Phys.* **1995**, *103*, 4807–4818.

(42) Xu, J.; Zhu, Z. Y.; Luo, S. Z.; Wu, C.; Liu, S. Y. *Phys. Rev. Lett.* **2006**, *96*, 027802.

(43) Zhu, Z. Y.; Armes, S. P.; Liu, S. Y. *Macromolecules* **2005**, *38*, 9803–9812.